EEET ECOLOGICAL ENGINEERING & ENVIRONMENTAL TECHNOLOGY

Ecological Engineering & Environmental Technology 2024, 25(7), 133–149
https://doi.org/10.12912/27197050/188266
ISSN 2719-7050, License CC-BY 4.0

Received: 2024.04.24
Accepted: 2024.05.14
Published: 2024.06.01

Use of Nano Co-Ni-Mn Composite and Aluminum for Removal of Artificial Anionic Dye Congo Red by Combined System

Reman A. Jasim[1], Rasha H. Salman[1*]

[1] Department of Chemical Engineering, College of Engineering, University of Baghdad, Baghdad, Iraq

* Corresponding author e-mail: rasha.habeeb@coeng.uobaghdad.edu.iq

ABSTRACT

The removal of congo red (CR) is a critical issue in contemporary textile industry wastewater treatment. The current study introduces a combined electrochemical process of electrocoagulation (EC) and electro-oxidation (EO) to address the elimination of this dye. Moreover, it discusses the formation of a triple composite of Co, Mn, and Ni oxides by depositing fixed salt ratios (1:1:1) of these oxides in an electrolysis cell at a constant current density of 25 mA/cm^2. The deposition ended within 3 hours at room temperature. X-ray diffractometer (XRD), field emission scanning electron microscopy (FESEM), atomic force microscopy (AFM), and energy dispersive X-ray (EDX) characterized the structural and surface morphology of the multi-oxide sediment. Marvelously, the deposition has simultaneously occurred on both anodic and cathodic graphite electrodes. These electrodes besides aluminum (Al) are employed as anodes in the EC-EO system, and the results were optimized by response surface methodology (RSM). The optimum operating conditions were a current density of 6 mA/cm^2, pH = 7, and NaCl of 0.26 g/L. The results showed that the combined system eliminated more than 99.91% of the congo red dye with a removal of chemical oxygen demand (COD) of around 97% with 1.64 kWh/kg of dye of the consumed energy. At low current density, the current delivered for the composite anode was more than for the Al anode with the same surface area. On top of this superiority, the EC-EO scenario is a practical hybrid process to remove CR in an environmentally friendly pathway.

Keywords: electrocoagulation, electro-oxidation, congo red, nanocomposite, aluminum, combined.

INTRODUCTION

The problems of water pollution with various chemical and biological substances are considered important and worrying issues, especially in recent years due to the great industrial revolution that took place in the world, which led to an increase in pollutants and harmful substances in the aquatic environment (Ahmed et al., 2020). Removing these pollutants or reducing their presence in the environment, to an acceptable percentage by using effective methods that can remove a contaminant quickly, efficiently, at low cost, constitutes a major challenge for scientists (Crini and Lichtfouse, 2019). A million tons of various types of impurities are thrown away daily into water drains, such as dyes, heavy metals, chemical fertilizers, organic compounds resulting from food production factories, or biological pollutants resulting from medical and pharmaceutical factories (Rathi et al., 2021).

Every day, more than 700,000 tons of various dyes are thrown into the water. A wide variety of industries make use of dyes, such as tanning and printing food industries (Inamuddin et al., 2021).

There are many types of dyes, some of which are natural and extracted from plants or insects, and others are manufactured. The process of manufacturing has been resorted to because of its importance and frequent use in various industries. Azo dyes are one of the most important and widely used types (Bafana et al., 2011).

Azo dyes are the most often employed synthetic dye; it is about 70% of all synthetic dyes worldwide each year. They have at least one azo group (-N=N-). In the absence of hydroxyl (OH^-),

sulfonic (SO_3^-), and other functional groups that pull electrons, these compounds are more resistant to breakdown by microbes. A variety of aromatic rings and chromophoric groups are possible in the azo dyes. Azo dyes are highly resistant to light and harsh environments due to their resonance and π-conjugated azo bond properties (Mahmoodi et al., 2018). Congo red (1-napHthalene sulfonic acid, 3,3′-(4,4′-bipHenylene bis (azo)) bis (4-amino-) disodium salt) is one type of azo dyes and it is utilized in plastic, paper, printing, rubber, and dyeing industries especially in textile industries because of its strong convergence with fiber (Ojo et al., 2019). CR is a complex aromatic dyes composed of benzidine and analogs can be toxic (Siddiqui et al., 2023). Research investigations have shown that congo red harms aquatic life and human health. Therefore, it needs to be removed or eliminated (Mandal et al., 2021). A lot of methods are used for dye degradation such as ion exchange (Jia et al., 2020), chemical precipitation (Shafqat et al., 2020), membrane separation (Tan et al., 2021), adsorption (Sabah and Alwared, 2019), and electrochemical processes (Ganash et al., 2023). The electrochemical processes have attracted great interest in recent years due to its advantages such as versatility, clean, and environmental acceptability characteristics. In general, electrochemical processes have no solid residual production, they apply electrons as a unique reagent and different methods of electrochemical are used for water purification such as electro-Fenton, electrocoagulation (EC), and electro-oxidation (EO), etc. (Ya et al., 2019). For eliminating suspended solids, collided material, heavy metal, and dyes, the EC process is used because it is efficient, friendless for the environment, and capable of treating large amounts of wastewater with low cost (Akhtar et al., 2020; Al-Qodah and Al-Shannag, 2017). Coagulants are produced from a sacrificial electrode such as aluminum and iron. Hydroxyl ions (OH^-) and hydrogen gas will be generated at the cathode due to water reduction (Beddai et al., 2022). The anode (M) will be dissolved and produce a metal cation as seen in Equations (1–3) (X. Chen et al., 2018).

$$M \rightarrow M^{n+} + ne^- \quad (1)$$

$$H_2O_{(l)} + 2e^- \rightarrow 2OH^- + H_2(g) \quad (2)$$

$$M^{n+} + n\,OH^- \rightarrow M(OH)_{n\ (s)} \quad (3)$$

Electro-coagulants will be produced because of the reaction between hydroxyl ion (OH^-) and metal cation M^{n+} to generate hydroxyl complexes which adsorb pollutant particles. The formed coagulants would be removed by the action of the flotation process with the help of H_2 and O_2 gases that are produced at the cathode, and anode, respectively (Al-Qodah and Al-Shannag, 2017; Criado et al., 2020).

Electro-oxidation is one of the most common techniques for purifying textile wastewater and other polluted water supplies (Abilaji et al., 2023), and it is classified into two types; direct oxidation and indirect electrooxidation. The direct oxidation process takes place on the anode surface as a result of the electron transfer. There are two types of electrodes and the efficiency of EO process depends on it. At the surface of the active electrode, the chemisorbed active oxygen (either, oxygen in the oxide lattice (MO_{x+1})) will selectivity oxidize the organic materials (R) as shown in Equation 4. While, at the surface of non-active electrodes, the physically adsorbed active oxygen (either, adsorbed hydroxyl radical ($OH^{\bullet}$) will completly oxidize the organic materials to water and carbon dioxide as shown in Equation 5. Therefore, it is preferred in oxidation processes such as boron-doped diamond (BDD), PbO_2, or Ti_4O_7 (Kapałka et al., 2007).

$$MO_{X+1} + R \rightarrow MO_X + RO + H^+ + e^- \quad (4)$$

$$MO(\bullet OH) + R \rightarrow CO_2 + H_2O + H^+ + e^- \quad (5)$$

The efficacy of every electrode was established based on its oxygen overpotential. High overpotential results in low oxygen evolution and elevated production of hydroxyl radicals, which are advantageous for breaking down organic components via direct electro-oxidation. For the anode, to generate the required amount of hydroxyl radical, its oxygen overpotential needs to be higher than 1.23 volts in comparison to the standard hydrogen electrode (SHE).

Indirect oxidation takes place by adding oxidation reagents like (H_2O_2, O_3, and NaCl). By adding NaCl, there are reactions would take place where hypochlorous acid (HOCl) or hypochlorite ion (OCl) can be formed as illustrated in Equations (6–8) (Nidheesh et al., 2018).

At anode: $2Cl^- \rightarrow Cl_2 + 2e^-$ (6)

At cathode: $2H_2O + 2e^- \rightarrow OH^- + H_2$ (7)

At bulk solution:

$$Cl_2 + H_2O \rightarrow HOCl + H^+ + Cl^- \leftrightarrow OCl^- + Cl^- + 2H^+ \quad (8)$$

Various types of electrodes were used for the EO process such as boron-doped diamond (BDD), PbO_2, platinum, IrO_2, graphite, and lead. Despite

these electrodes having many utilizations, they also have several drawbacks, such as being costly, easily broken, or non-reactivable (Li et al., 2021; Moreira et al., 2017). To avoid these problems, several metal oxides were deposited on the surfaces of the substrates to produce a wide variety of two and three-dimensional composites, which can be accomplished with electrodeposition process, which is a versatile and inexpensive process. An understanding of electrochemical processes about the reduction or deposition of electroactive and accompanying species on the surface of the electrode forms the basis of the electrodeposition process. By considering the electrochemical principles into consideration for specific applications and purposes, the electrodeposition process might be made more controlled. The design and control of electrodeposition processes are influenced by numerous empirical aspects such as voltage utilized, temperature, time of deposition as well as the composition of the electrolyte (Kul et al., 2020). Numerous metal oxides gained attention like nickel oxides which have gained great importance in improving electrode performance and increasing energy storage capacity (Chen et al., 2020). Cobalt oxide has a good characteristic because it enhances the surface area, facile electrode construction, and satisfactory chemical stability (Nare et al., 2022). A significant advantage for manganese oxide arises from its low cost and catalytic activity which increases its efficiency (Sergienko and Radjenovic, 2020). The efficiency of MnO_2, PbO_2, and Co-Mn-Ni oxides in removing phenol was investigated by previous studies (Abbas and Abbas, 2022; Ahmed and Salman, 2023a). Besides, some previous studies investigated the efficiency of dye removal combined with an EC-EO- system (Chakchouk et al., 2017; Chanikya et al., 2021) which illustrated that these systems reduce cost and time besides their high efficiency. The present research aims to evaluate the effectiveness of the combined EC-EO process to remove congo red dye from an aqueous solution. Our approach involves simultaneous depositing of nano cobalt, manganese, and nickel oxides onto cathodic and anodic graphite substrates with a fixed molar ratio of these metal salts. The prepared nano oxides would be utilized as the anode for the EO process besides Al as the sacrificial electrode for the EC process in the same electrolytic cell with three stainless steel electrodes as auxiliary electrodes. To optimize the removal efficiency of congo red, in a batch system, three parameters (pH, current density, and NaCl concentration) would be investigated with the surface response method. A comparison between EC system, EO system, and combined EC-EO system would be accomplished to predict the difference in effiency between single and combined systems.

EXPERIMENTAL WORK

Methods and materials

Distilled water was used in the preparation of all aqueous solutions, all chemicals used in experiments were of reagent grade, and there was no need for further purification. These chemicals were: $Ni(NO_3)_2 \cdot 6H_2O$ (with a purity of 99.0%, Central Drug Hense), $MnCl_2 \cdot 4H_2O$ (with a purity of 98.0%, Techno PHarmchem), $Co(N0_3)_2 \cdot 6H_2O$ (with purity 97%, THOMAS BAKER), HCl (37%, liquid, Sigma-Aldrich), Congo red (with a purity of 99.0%, ANJDULY), NaCl (with purity of 99.5%, Avonchem), NaOH (pellets with purity 98%, ALPHA CHEMIKA), and Na_2SO_4 (with purity 99%, LOBA CHEMIE).

Electrodes preparation

15 cm long, 5 cm wide, and 0.3 cm thick of graphite substrates which were utilized as the anode and cathode in the electrodeposition cell were activated before electrodeposition experiments, the surface needs to be polished and purified before use. The initial step involves heating the substrate to 350 °C in a (N20/H W-Germany) furnace for 30 minutes. This process removes any impurities or oxide layer presented on the substrates. Then, the surface was polished with 320-grit sandpaper and then immersed in acetone for more purification. Finally, the electrode was washed with distilled water.

Synthesis of (Co-Mn-Ni) nano metal oxide electrode

Deposition of nano metal oxides onto the cathode and anode was simultaneously carried out with a constant current density of 25 mA/cm^2. For the deposition of nano metal oxides on two (5 cm×15 cm×0.3 cm) graphite sheets, a batch electrolytic cell was used and 3 cm gap between the two electrodes was kept and 50 cm^2 as an active area of graphite substrate was immersed inside an electrolyte containing 0.075 M of $Co(NO_3)_2 \cdot 6H_2O$, $MnCl_2 \cdot 4H_2O$, and $Ni(NO_3)_2 \cdot 6H_2O$ with a fixed molar ratio (1:1:1).

These metal salts were dissolved in 0.35 L of distilled water at room temperature 27 °C ± 1, and the deposition experiment continued and for 3 h (1.5 for each side) without stirring (Ahmed and Salman, 2023b).

After the electrodeposition process, the cathode and anode were rinsed with distilled water, and the composite electrodes were allowed to dry at room temperature for 24 h. The efficiency of prepared electrodes (cathode and anode) was investigated in a combined EC-EO system to eliminate Congo red dye by utilizing them as anode for the (EO) process. Surface structure and crystal size was analyzed by XRD analytical X' Pert Pr (UK). Diffraction data was obtained at 2θ by using Cu-Kα radiation (λ=1.5406 °A), with a voltage of 40 kV, and a current of 30 mA from 10° to 80°. FESEM (field emission scanning electron microscopy-imaging-EDS-Mapping-Line EBSD-Germany with 25 KV) was used and EDX was utilized to determine its chemical composition and weight percentage. To examine the mean diameter and roughness of the Nano oxide layer deposited on the graphite surface, AFM (AFM/SPM dual Scope TM-DS) was utilized. The deposited cathode would be identified as (A1) and the deposited anode was identified as (A2).

Oxygen overpotential measurement

Electrodes and their types are considered the governing and influential element in water treatment by electrochemical technique. In the EO process, oxygen overpotential is crucial because it determines the value of the excess voltage controlling the evolution of oxygen from the anode (Wu et al., 2014). To detect the oxygen overpotential for each composite electrode (cathode and anode), the process was achieved by comparing the oxegen overpotential on nano metal oxide electrodes with the overpotential of standard hydrogen electrode (SHE). Three-electrodes in an electrolytic cell were utilized for electrochemical measurement. A stainless steel electrode was used as a counter electrode and a standard hydrogen electrode (SHE) as the reference electrode while the nano composite electrode was the anode. All potential measurements were taken in an aqeous solution of 200 mg/L of CR besides 0.02M of Na_2SO_4 or 0.02M of Na_2SO_4+ 0.5 g/L of NaCl and a current density under 6 mA/cm^2 was applied.

Combined EC-EO system

Simultaneous removal of congo red was accomplished by combining EC with EO processes at the same cell, in a perspex batch reactor. All electrodes had the same width and length (5×15) cm^2, three of them were stainless steel plates (type 316, with 0.3 cm thickness) utilized as cathodes, and an Al electrode with 0.4 cm thickness as a sacrificial anode for the EC process. While, for the EO process, the composite electrode with (Co-Mn-Ni) Nano metal oxide was employed, the active area for each face of the anodes was 25 cm^2 and the total active area was 100 cm^2 for the two anodes (Al and composite) with a 2 cm distance between each two electrodes. All electrodes were connected in a monopolar manner to the digital power supply type (MAISHENG MS-605D) and were fixed vertically inside the cell by a perspex cover that has seven slots, five for fixing electrodes and two holes for pH probe (OHAUS Corporation, USA) and mercury thermometer probe. To ensure that the mixture is thoroughly mixed, the electrolytic solution was stirred with a magnetic stirrer (Heidol pH™ 505-20000-00, 0–300 °C; 0–1400 rpm) at 250 rpm, Figure 1 shows the schematic diagram of the electrochemical system. For each run, 200 mg/L of congo red dye was dissolved in 2 L of distilled water. Before each removal experiment, the pH value was adjusted by 0.1M of hydrochloric acid (HCl) and 0.1M of sodium hydroxide (NaOH). A 0.02 M of Na_2SO_4 was added to improve solution conductivity, lower voltages and reduce energy consumption; it raised the conductivity of simulated congo red solution from 0.38 to 4 mS/cm, and this conductivity measured by a conductivity meter (HANNA, Romania). In all runs, samples were taken before the operation and after 20 minutes from electrolysis where 10 ml of solution was taken and left for one hour to precipitate, and to determine the concentration of dye in the electrolyzed solutions a UV-Vis-9200 (Biotech Engineering Management Co. Ltd. (UK) was utilized by detecting the light absorption of congo red complex at λ = 494 nm. The removal efficiency of congo red was calculated by Equation 9 (Ali and Mohammed, 2020), where C_i and C_f are the initial and the final dye concentration in mg/L.

$$Congo\ red\ dye\ removal\ \% = \frac{(C_i - C_f)}{C_i} \times 100 \quad (9)$$

To ensure that the combine (EC-EO) process is efficient in removing organic components not only color, COD in mg/L was examined at optimum conditions by a COD reactor (Lovibond® Water Testing, MD 200 COD, tube testing, Germany). A 2 ml of treated sample was mixed with potassium dichromate in a tube and oxidized at 150 °C for 2 h, cooled

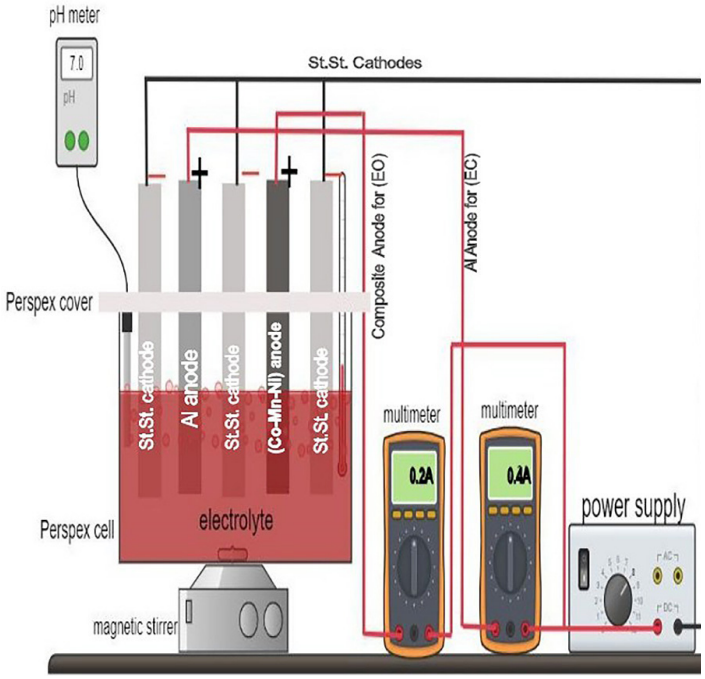

Figure 1. A Schematic diagram of the combined EC-EO cell

at room temperature, and measured by Photometer-System MD200 (Lovibond® Water Testing, Thermo reactor RD 125, Germany). COD efficient removal % was calculated by the following Equation (Sathishkumar et al., 2019).

$$COD\ removal\ \% = \frac{Initial\ COD\ conc. - final\ COD\ conc.}{Initial\ COD\ conc.} \times 100 \quad (10)$$

For every kilogram of dye, the quantity of energy consumed in the process was represented by the specific energy consumption (SEC), Equation 11 can be used to obtain consumed energy in kWh/kg of congo red (Zou et al., 2017).

$$SEC = \frac{E.I.t}{(C_i - C_f)\,V} \times 1000 \quad (11)$$

where: *SEC* is the energy consumption in (kWh/kg of dye), *E* indicates voltage in (Volt), *I* represents the current applied in (ampere), *t* indicates electrolysis time in (h), v represents the volume in (L), and C_i, C_f represent the initial and final dye concentration, respectively.

Experimental design

Response surface method (RSM) deals with multiple variables, the most used types in design processes and analysis of experiments are central composites and Box-Behnken designs. A Box-Behnken (BB) experimental design involving 15 experiments was used in recent work, with a center point and three duplicates. A BBD is a type of order-scalable rotational design that is commonly used to improve the effectiveness and efficiency of experimental designs (Ruoho et al., 2020). A set of experiments was conducted to predict the optimal conditions for the removal process; three parameters were chosen to be examined; pH, current density, and NaCl concentration. Table 1 illustrates the levels of the investigated parameters; *X*1 is pH (5, 7, 9), *X*2 is current density (2, 4, 6) mA/cm^2, and *X*3 as NaCl concentration (0, 0.25, 0.5) g/L, 20 min was used as electrolysis time for all runs. Minitab software version-19 was used to analyze the experimental results which were fitted with the second-order Equation as shown in Equation 12.

$$Y = b_0 + \sum b_i x_i + \sum b_i i x^2_i + \sum b_{ij} x_i x_j \quad (12)$$

where: *Y* is congo red dye removal %, b_0, b_i, and b_j are regression coefficients.

Table 1. Level of variables of BBD experimental design

Independent variable	Level		
	-1	0	1
X1 (pH)	5	7	9
X2 (C.D, mA/cm^2)	2	4	6
X3 (NaCl, g/L)	0	0.25	0.5

RESULTS AND DISCUSSION

Electrodes characterization

XRD analysis

The crystal structure of Co-Mn-Ni nano metal oxides that are deposited on the surface of the cathode and anode can be observed in Figure 2. Different types of oxides were performed on the electrodes, the peaks that can be detected are in good agreement with the graphite substrate and the usual cubic phase of CoO (JCPD card No.-075-0533), the peaks of CoO that correspond to hkl of (111, 200, and 400) were at 2θ = 37.33°, 42.6° and 44.85°, respectively. NiO cubical structure was detected onto cathode and anode at 2θ of 37.33° and 42.57° which correspond to hkl 111, and 200, respectively; this result agrees with JCPD standards No.075-01017. However, tetragonal Mn_3O_4 was detected at 2θ peaks (26.62°, 37.33°, 43°, 54.67°, 77.88°, 44.8°, and 77.81°) that match with hkl of (211, 213, 400, 413, 444, 400, and 435), respectively which agree with (JCPDS-card No. 075-1560). To calculate the crystal size of the deposit partials, the Scherrer Equation was used as follows (Ruoho et al., 2020):

$$Crystal\ size = \frac{k \times \lambda}{\beta\ cos\theta} \tag{13}$$

where: λ is the X-ray wavelength (1.5404 °A), β is the line broadening at half the maximum intensity (FWHM), K is the dimensional shape factor of about 0.9, and θ is Bragg angle.

Based on the results of the determined crystal size of the cathode and anodes, it was revealed that the crystal size of the cathode was larger than that of the anode, which was 27.67 nm for the cathode, and 18.07 nm for the anode that's because of hydrogen gas evolution at the cathode, which caused aggregation of particles together and increasing in the growth rate. The prepared anodes showed an amorphous layer of Co-Mn-Ni oxide, whereas the prepared cathodes showed a crystalline structure.

FESEM analysis

Figure 3 shows the morphological structure of the deposited cathode (A1) and deposited anode (A2) with two magnifications (50 000× and 10 000×). Nano spheres which were gathered to give structure like flowers were revealed at the

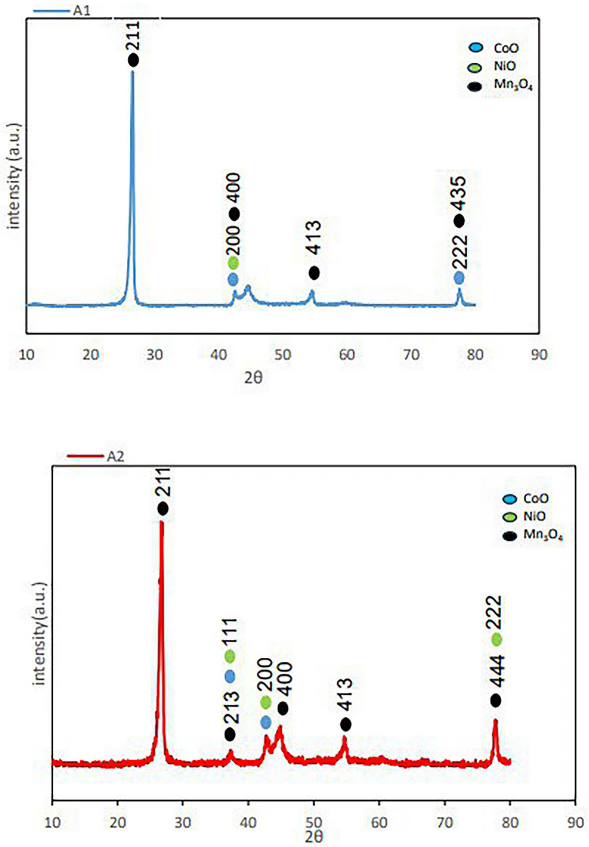

Figure 2. XRD for (Co-Mn-Ni) Nano oxide deposit on the cathode (A1), and anode (A2) at 0.075M concentration with constant molar ratio (1:1:1), current density = 25 mA/cm^2, within 3 h.

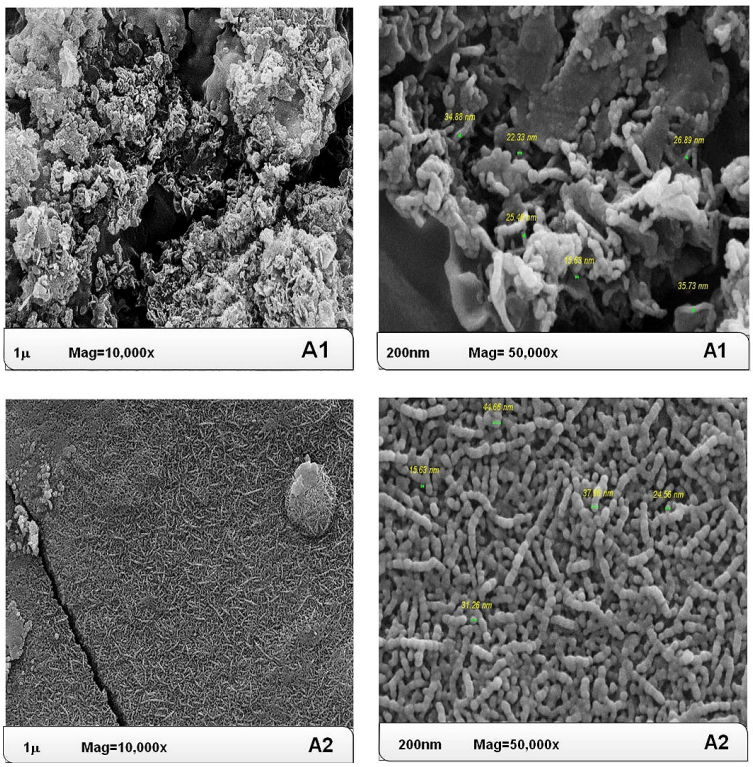

Figure 3. FESEM image of (Co-Mn-Ni) at different magnifications (50 000×, 10 000×) for cathode (A1), and anode (A2) prepared with fixed molar ratio (1:1:1), 25 mA/cm^2, within 3 h.

cathode A1 and this result is in agreement with the previous study by (Abbas and Abbas, 2022). This granular complex structure occurred on the cathode surface giving it more porosity, more active sites, and high efficiency of ions transport in electrolytes, which would promote electrolyte diffusion while lowering internal resistance (Li et al., 2018). The anode showed a striking black color, while the cathode had a greenish color.

The anode A2 is shaped like a rod which consists of a complex network of clustered spheres. Block structure was observed on its surface because oxidation and deposition occurred together on the anode. This structure demonstrated that the electrode can undergo oxidation and deposition of metal ions simultaneously, and this is what gave the anode a flat shape, and this agrees with previous research. Some cracks have appeared on the surface, and the reason may be the temperature difference between the electrolyte and the water used for rinsing or during drying (Abbas and Abbas, 2019).

EDX analysis

EDX analysis was conducted to confirm the presence of Co, Mn, Ni, and O on the cathode and anode surfaces as shown in Table 2. The analysis revealed that Ni was predominantly deposited on the cathode surface (as seen in Table 2), while Mn was mainly found on the anode surface. On the other hand,Co had moderate deposition on the electrodes.

The difference in the rates of ion deposition on the surfaces of the cathode and anode is due to several reasons, including the speed of metal dissolving on the cathode and redox potential on the anode which has also been noticed in previous research (El Boraei and Ibrahim, 2019).

AFM analysis

AFM analysis was used to examine the topography of the deposit Co-Mn-Ni. Nano oxides on cathode and anode and the results are presented in Figure 4. It is widely accepted that the surface roughness of electrodeposited nanomaterials is often associated with grain size (John et

Table 2. EDX element analysis for (Co-Mn-Ni) nano oxide electrode

Element component	Cathode	Anode
	Wt.%	Wt.%
Ni	33.1	6.3
Co	23.6	10.1
O	33.6	38.5
Mn	9.7	45.1

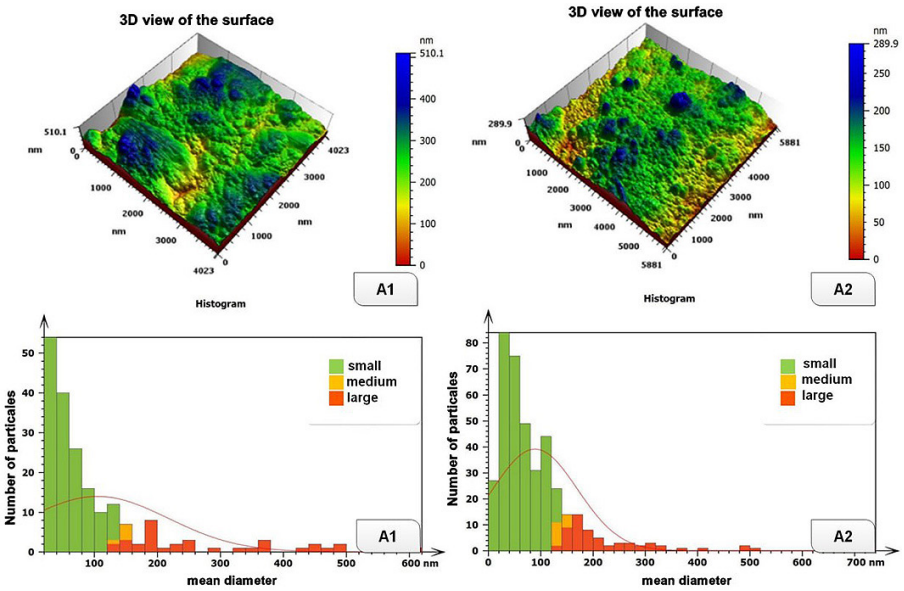

Figure 4. AFM images, particle size, and granularity accumulation of (Co-Mn-Ni) nano oxides deposit on the cathode (A1) and anode (A2) at 0.075 M concentration with fixed molar ratio (1:1:1), current density 25 mA/cm^2 within 3 h

al., 2023). As seen in Figure 4, the distribution of granularity represented the accumulation of particles with the average mean diameters. The average mean diameter for the cathode and anode was 104.8 nm and 89.19 nm, respectively. The roughness (root mean square) of the Nano oxide layer on the cathode and anode was 76.68 nm and 46.16 nm, respectively. From the result of the root mean square, it was observed that the cathode had more roughness than the anode, and this roughness was caused by the hydrogen gas generation on the cathode surface.

Electrochemical characterization of electrodes

From Table 3 which represents the oxygen overpotential for the prepared cathode and anode, electrodes detect high overpotential in 0.02M of Na_2SO_4 with and without NaCl salt higher than1.23 vs. SHE for direct oxidation and 1.64 vs. SHE for indirect oxidation which proved that (Co-Mn-Ni) nano metal oxides enhanced the properties of the graphite substrate in an electrochemical process and improved its efficiency in water treatment because electrodes with high overpotential cause complete oxidation of organic components (Wu et al., 2014). It was approved that if electrodes were prepared by electrodeposition and decomposition, then they would have higher oxygen overpotential than those prepared by the thermochemical methods. Moreover, the time required for the electrodeposition process contributed in the rising potential of the electrode where longer time of deposition means more oxide layer coated the electrode (Chen et al., 2010).

STATISTICAL ANALYSIS

Development of regression model

Data of actual and predicted congo red elimination efficiency as well as energy consumption (SEC) after 20 min of electrolysis are presented in Table 4. The lowest removal was 75.8% and the highest removal was 98.8%. The regression model equations obtained with MINITAB-19 software as shown in the following Equation.

Table 3. Oxygen overpotential for (Co-Mn-Ni) composite electrodes (cathode and anode) in a fixed molar ratio (1:1:1)

Aqueous solution	Oxygen overpotential (V)	
	composite cathode	composite anode
0.02 M Na_2SO_4, 0 g/L of NaCl	2.98	2.96
0.02 M Na_2SO_4 + 0.5 g/L of NaCl	2.38	2.44

Table 4. Actual and predicted values for congo red removal% and energy consumption (SEC)

Runs	pH, (X1)	C.D (mA/cm^2), (X2)	NaCl conc. (g/L), (X3)	Actual congo red removal %	Predicted congo red removal%	E (V)	SEC (kWh/kg) congo red
1	7	4	0.25	97.5	97.585	3.4	1.173
2	5	4	0	79.802	79.603	3.3	1.357
3	7	6	0.5	98.897	97.537	3.5	1.681
4	9	2	0.25	88.327	88.153	2.5	0.469
4	5	2	0.25	84.018	82.858	2.2	0.818
6	7	4	0.25	97.649	97.585	3.4	1.191
7	7	4	0.25	97.607	97.585	3.5	1.220
8	9	6	0.25	95.461	96.621	3.3	1.574
9	9	4	0.5	90.541	90.740	2.7	0.897
10	7	2	0.5	93.986	93.960	2	0.347
11	9	4	0	85.314	84.128	3.4	1.231
12	7	6	0	96.559	96.5858	3.7	1.913
13	7	2	0	75.845	77.205	2.4	0.513
14	5	4	0.5	89.510	90.696	2.7	0.989
15	5	6	0.25	97.174	97.348	3.4	1.650

$$\begin{gathered} \textit{Congo red removal } \% = \\ -22.6 + 22.54\,X1 + 9.79\,X2 + 109.9\,X3 \\ -1.421X1^2 - 0.164X2^2 - 89.7X3^2 - \\ 0.376X1X2 - 2.24X1X3 - 7.90X2X3 \end{gathered} \quad (14)$$

where: $X1$, $X2$, and $X3$ are pH, current density, and NaCl conc., respectively.

Analysis of variance (ANOVA)

Identifying the impact of variables and their interactions on the response can be predicted by ANOVA, which is an effective tool for process optimization and understanding. Table 5 shows the results of ANOVA, Cont.% represents the contribution percentage of parameters, Seq.SS is the Sequential Sum of Squares, Ad j.MS stands for Adjusted Mean Squares, P value is the probability value and F-value is the Fisher value, high F-value (more than 4) means that the regression Equation can adequately explain the variation in the response. If the p-value is less than 0.05, the model has been considered statistically significant (Özyurt et al., 2017). Table 5 shows that the model for congo red degradation was highly significant with F and P values of 43.09 and 0.000, respectively, and that the model can describe the removal process efficiently. High value of correlation coefficient R^2 (98.73) was obtained, and the contribution percentages results revealed that current density had the highest influence on the congo red removal followed by NaCl conc., and pH.

Effect of studied parameters on congo red dye removal

To study the effect of each operating parameter on the removal efficiency of congo red, a 3D surface plot based on RSM analysis and histogram plot would be conducted. The effect of pH and current density on the congo red dye removal at 0.25 g/L of NaCl can be detected in Figure 5. From the 3D plot, it can be observed that an increase in current density has a high effect on dye removal, increasing the current density led to an increase in removal efficiency. For example, the results of Table 4 showed that at pH 5 and NaCl 0.25 g/L, congo red dye removal increased from 84.018% to 97.17% as the current density increased from 2 to 6 mA/cm^2. In comparison, it increased from 93.98% to 98.89% when current density increased from 2 to 6 mA/cm^2 at pH=7 and 0.5 g/L of NaCl within 20 min of electrolysis.

The importance of the current density effect due for two reasons; first, its effect on the EC process, where at high currents, the dissolution of the aluminum anode electrode increases which causes a release of a greater number of metal ions in the electrolyte according to Faradays' law (m = [*ItM*/*zF*]). On the other hand, more species of hydroxyl ions (OH^-) generation would be obtained due to the hydrolysis of water

Table 5. ANOVA results for congo red removal

Source	DF	Seq SS	Cont.%	Adj SS	Adj MS	F-value	P-value
Model	9	726.003	98.73%	726.003	80.667	43.09	0.000
Linear	3	430.733	58.57%	430.733	143.578	76.70	0.000
pH	1	10.438	1.42%	10.438	10.438	5.58	0.065
C.D	1	263.531	35.84%	263.531	263.531	140.78	0.000
NaCl conc.	1	156.764	21.32%	156.764	156.764	83.74	0.000
Square	3	218.750	29.75%	218.750	72.917	38.95	0.001
pH*pH	1	102.423	13.93%	119.342	119.342	63.75	0.000
C.D*C.D	1	0.186	0.03%	1.585	1.585	0.85	0.400
NaCl conc.* NaCl conc.	1	116.141	15.79%	116.141	116.141	62.04	0.001
2-way interaction	3	76.520	10.41%	76.520	25.507	13.63	0.008
pH*C.D	1	9.068	1.23%	9.068	9.068	4.84	0.079
pH* NaCl conc.	1	5.020	0.68%	5.020	5.020	2.68	0.162
C.D*NaCl conc.	1	62.432	8.49%	62.432	62.432	33.35	0.002
Error	5	9.360	1.27%	9.360	1.872	–	–
Lack-of-fit	3	9.348	1.27%	9.348	3.116	526.21	0.002
Pure error	2	0.012	0.00%	0.012	0.006	–	–
Total	14	735.362	100.00%				
Model summary	S	R-sq	R-sq (adj.)	PRESS	R-sq (pred.)		
	1.36819	98.73%	96.44%	149.592	79.66%		

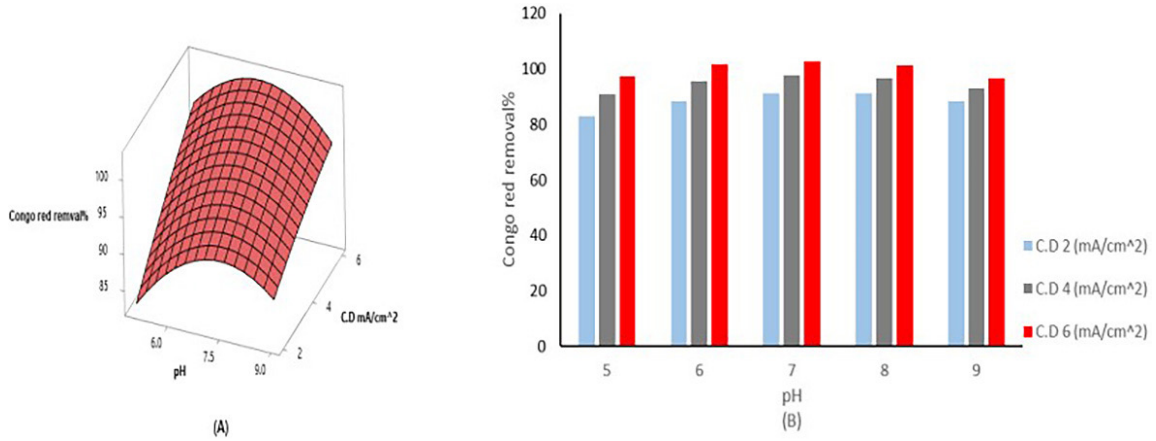

Figure 5. Effect of current density with pH on congo red dye removal% (NaCl conc.= 0.25 g/L, C_i = 200 mg/L, time 20 min, temperature = 25 ± 2 °C), (a) 3D surface plot, (b) histogram plot

on the cathode surface, and this resulted in the production of more collided particles or metal hydroxide $Al(OH)_3$. These metal hydroxyl particles led to the destabilization of the dye atoms and their aggregation (Mousazadeh et al., 2023). This aggregation continued and the agglomerations grew, causing large flocks according to Brownian motion which would facilitate the process of flotation and precipitation of Congo red dye. The second effect of current density is on the EO process; in direct oxidation when an increase in the generation of oxidized radicals ($OH^{\bullet}$) results on the anode surface, and in indirect oxidation, the dissolve of chlorine ions increases, and more HOCl and OCl^- would be produced in the electrolyte, similar results have appeared in previous studies (Periyasamy and Muthuchamy, 2018). Another reason for the increase in removal efficiency with increasing current is the amount of hydrogen gas produced on the surface of the cathode. This resulting a high number of bubbles which causes higher mass transfer, high speed in

the flotation of the collected particles, and ease of disposal (Kul et al., 2022). Table 5 illustrates the low effect of pH on the removal efficiency with a 1.23 of contribution percentage. The effect of pH can also be observed in Figure 5, the highest removal percentage of Congo red was obtained at pH =7 and the lower values of removal efficiency were obtained at alkaline and acidic conditions. This can be attributed to the fact that various types of Al ions can be produced based on pH value. At pH from (5–8), $Al(OH)^{+2}$, $Al(OH)_2^{+}$, $Al(OH)_3$, $Al_2(OH)_2^{+4}$, and $Al_{13}(OH)_{32}^{+7}$ are produced which have a high positive charge which causes adsorption of a neutralization reaction. At pH more than 9, $Al(OH)_4^-$ increased and the positive charge of $Al(OH)_3$ decreased and hypochlorite ion (OCl^-) appeared which has a low ability of oxidation in comparison with hypochlorous acid (HOCl) that appeared at acidic and neutral electrolyte (Kabdaşlı and Tünay, 2023; Nasr et al., 2016; Turan, 2021).

The effect of NaCl with current density on the removal of 200 mg/L of congo red is shown in Figure 6 at pH = 7 and after 20 min of electrolysis. It can be observed that increasing current density from (2–6) mA/cm^2 leads to an increase in the breakdown of the congo red dye in the presence or absence of NaCl salt, but adding NaCl improves electrical conductivity and reduces energy consumption. It also decomposes and produces HOCl, which is considered a strong oxidizer as shown previously in Equation 8. As can be seen from Figure 6b, at a current density of 4 mA/cm^2 and without adding NaCl, the removal efficiency is 87.55%. The removal increases with the addition of NaCl and reaches the high value of 98.275% at NaCl = 0.25 g/L. When NaCl increases more than 0.25g/L, the removal efficiency begins to decline even though a high concentration of NaCl is supposed to improve the removal process because it prevents the passive layer from growing on the anode surface. But, in a combined (EC+EO) system a different behavior could be noticed and the reason could be that excess of chlorine ions has a complex attracted with Al^{+3} ions, and that leads to reduce the precipitate of positive charge on aluminum hydroxide which affects metal ions diffusion and dye adsorption or it caused corrosion in the composite electrode (Co-Mn-Ni) and caused a lose in the layer of coalesced oxides and active site and low productivity, a similar finding was observed in previous studies (Periyasamy and Muthuchamy, 2018; Salman and Abbar, 2023).

In Figure 7, the impact of NaCl and pH on congo red removal is shown. At a current density of 4 mA/cm^2 and pH= 7, when NaCl increased from (0–0.5) g/L, the removal efficiency was 87.55% and 98.27%, respectively, due to the release of HOCl (strong oxidation agent) and the increase in the conductivity of the electrolyte which caused faster ions transfer in the presence of NaCl. Congo red degradation at pH 7, 9, and 5 were 98.27%, 93.52%, and 91.64%, respectively, and this is due to the formation of different types of metal ions depending on the value of pH. From Figure 7b, it can be concluded that at pH = 7, NaCl 0.25 g/L, and 4 mA/cm^2, the congo red removal efficiency was > 97%, the same behavior was observed by other researchers (Periyasamy and Muthuchamy, 2018; Salman and Abbar, 2023).

As expected, the results of consumed energy (SEC) showed that it increased with current

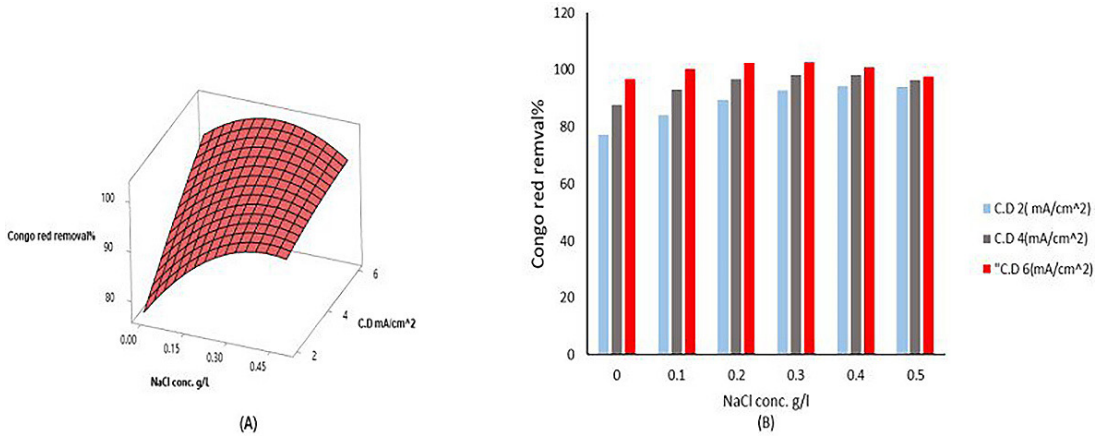

Figure 6. Effect of current density with NaCl conc. on congo red dye removal, C_i = 200 mg/L, pH=7, time 20 min, temperature = 25 ± 2 C°, (a) 3D surface plot, (b) Histogram plot.

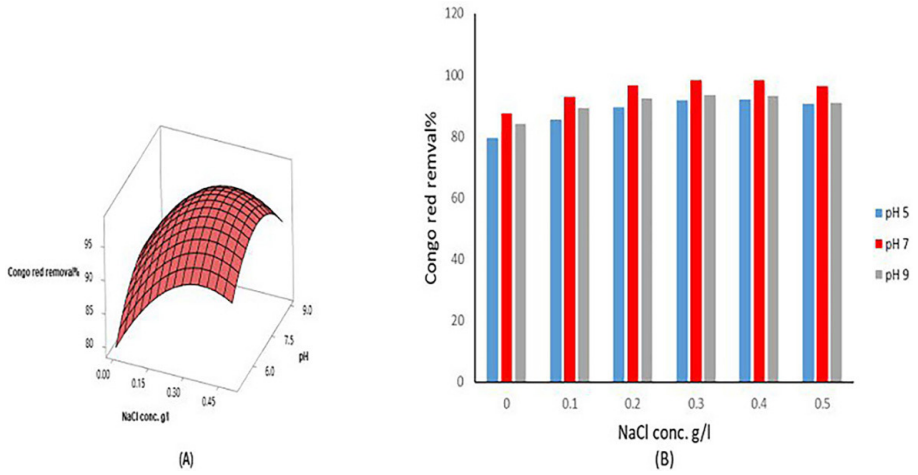

Figure 7. Effect of NaCl with pH on congo red dye removal% (current density= 6 mA/cm^2, C_i = 200 mg/L, time = 20 min, temperature = 25 ± 2°C), (a) 3D surface plot, (b) histogram plot.

density increasing. For example, by increasing current density from 2 to 6 mA/cm^2 at pH = 7 and 0.5g/L of NaCl, the consumed energy increased from 0.3473 to 1.6808 kWh/kg of dye. While increasing NaCl concentration led to a decrease in the value of consumed energy which it can be observed in Table 3, it decreased from 1.357 to 0.989 kWh/kg of dye at 4 mA/cm^2, pH = 5 as NaCl concentration increased from 0 to 0.25 g/L, respectively. This can be attributed to the fact that increasing NaCl concentration would enhance the conductivity of the electrolytic solution, decrease the voltage, and decrease the consumed energy as a result. Furthermore, it was observed that current density was not divided equally between electrocoagulation and electro-oxidation processes, either between Al and Co-Mn-Ni anodes, and it depended on the value of current density. At the low value of current density, the EO was the dominating process in the EC-EO combined process which means that Co-Mn-Ni anode took higher values of current density in comparison with Al.

The optimization and confirmation experiments

In all electrochemical systems, to achieve the main goal of treating wastewater and removing pollutants with the minimum consumed energy, optimizing several parameters to reach maximum removal with the least energy and cost is the main goal. Minitab-19 was used to reach to the main objective by expanding the desirability function (DF) using regulating weight or importance, this is classified into five factors minimum, maximum, target, in range, and nothing (Chakawa and Aziz, 2021; Theydan et al., 2024).

As the purpose of our system is to reach the highest efficiency of congo red removal, the maximum target was used in Table 6a, and the actual lower and upper results of Congo red removal were 75.854% and 98.897%, respectively. In Table 6b, optimum parameters from the desirable function were pH of 6.96, current density of 6 mA/cm^{2,} and 0.26 g/L of NaCl. Two experiments were conducted by applying optimum parameters, and the result is shown in Table 7. Average congo red removal efficiency was 99.91% after 20 min and COD removal % was measured at these optimum conditions and it was 97%. This result is near the range of optimum value in Table 6, that indicating Box–Behnken system and desirable function (1) succeeded in analyzing the combined EC-EO system for congo red removal.

Comparative to previous studies

In previous studies, congo red dye was eliminated by using the EO process or EC process only. Sathishkumar et al. (2019) achieving 98% of 100 mg/L of congo red via EO process after 10 min with 20 mA/cm^2 of applied current density, pH= 7, and 2 g/L of NaCl by using electrode RuO_2-IrO_2 coated titanium electrode.

By using the EC process, Mohammadlou et al. (2014) removed 98% of 50 mg/L of congo red, after 5 min by applying 15 mA/cm^2, pH= 7.5, and 10 g/L of NaCl. No comparison between using each method (EC and EO) alone in the process of treating congo red in earlier works (Kaur and Kaur, 2016; Ramya Sankar and Sivasubramanian,

Table 6. Optimum result for maximum congo red removal system (a) actual result, (b) multiple response prediction

a)	Response	Goal	Lower	Target	Weight	Importance		
	Actual congo red removal%	maximum	75.854	98.897	1	1		
b)	pH	Current density (mA/cm)	NaCl conc. (g/L)	Fit	SE fit	95% CI	95%PI	Composite desirability
	6.93	6	0.26	102.687	0.861	100.473,104.9	98.531–106.843	1

Table 7. Approval of optimum congo red removal efficiency

Run No.	pH	Current density (mA/cm^2)	NaCl conc. (g/L)	Congo red removal%	E (Volt)	Average removal%	SEC (kWh/kg of cong red)
1	6.96	6	0.26	100	3.5	99.91	1.533552632
2	6.96	6	0.26	99.82	3.7		1.759728064

Table 8. Primary experiment for EC, EO, and combined (EC+EO) at pH 7, 0.25 g/L of NaCl, 4 mA/cm^2 within 20 min

Applied system	C.D (mA/cm^2)	NaCl conc. (g/L)	pH	Congo red dye removal %
Only EC with two Al electrodes as anodes, and 3 st.st. electrodes as cathodes	4	0.25	7	80
Only EO with two Co-Mn-Ni electrodes as anodes, and 3 st.st. electrodes as cathodes	4	0.25	7	45
Combined (EC with Al electrode + EO with graphite electrode, and 3 st.st. electrodes as cathodes)	4	0.25	7	84
Combined (EC with Al as anode + EO with Co-Mn-Ni as anode), and 3 st.st. electrodes as cathodes)	4	0.25	7	98

2020). In terms of the applied current, the amount of salt added, and the time required for removal, the present work with a combined system succeeded in shortening the time and consumed energy and achieving a high removal for high concentrations of congo red by using low current density with a few amounts of NaCl.

To prove the effectiveness of the combined process with the Co-Mn-Ni composite electrode and to prove its enhancement in removing the congo red, a set of preliminary experiments were conducted with 200 mg/L of congo red, and 4 mA/cm^2 current density was applied, pH =7, and 0.25g/L of NaCl as supporting electrolyte was added within 20 min of electrolysis in all experiments. First, only electrocoagulation (EC) was accomplished using two sacrificial aluminum electrodes. As shown in Table 8, 80% of removal was obtained after 20 minutes. In contrast, 45% removal efficiency was achieved when two composite electrodes were used as anodes of the EO process only. Then the combined EC-EO system with Al and graphite electrode as anodes gave 85% of dye degradation. However, when using the combined system (EC with Al + EO with the Co-Mn-Ni composite electrode) under the same conditions, the removal rate reached 98%.

These results indicated that the combined method effectively removes Congo reed with high removal rates.

CONCLUSIONS

A combined EC-EO batch cell was used for the elimination of congo red dye, an Al electrode was used as the sacrificial anode for the EC process, and a Co-Mn-Ni composite electrode which was prepared by electrodeposition process used as the anode for the EO process. In electrodeposition process, 0.075 M from cobalt nitrite, nickel nitrite, and manganese chloride was utilized to deposit Co, Mn, and Ni oxides on a graphite substrate at 25 mA/cm^2 within 3 h. XRD, FESEM,

EDX, and AFM analyses proved the formation of (Co-Mn-Ni) nano metal oxides on the surfaces of the cathode and anode with 27.64 and 18.07 nm of crystal size, respectively. The average mean diameter for the cathode was 104.8 and 89.19 nm for the anode, respectively. The deposits of nano-metal oxide enhanced the efficiency of graphite electrodes for dye removal, with high stability, and corrosion resistance. The deposited Co-Mn-Ni oxides onto the cathode and anode have identical and very close efficiency in dye removal. The results of BBD and the result optimization of parameters showed that 99.91% and 97% of congo red removal% and COD removal%, respectively was achieved with energy consumption of 1.647 kWh/kg of dye in 20 minutes at the optimum process conditions (pH= 6.96, 6 mA/cm^2, and 0.2626 g/L of NaCl). ANOVA results showed that the sequence effect of parameters was current density > NaCl > pH. It was perceived that current density was not divided equally between the Al and Co-Mn-Ni electrodes, and it depended on the value of current density, at the low value of current density, the EO was the dominating process in the EC-EO combined process. Compared with the results of previous studies, the combined system (EC+EO) succeeded in the congo red dye removal process with high effectiveness and low energy consumption within a short period in comparison to the EC process alone, EO process alone, and EC+EO with Al and graphite anodes. Besides, the composite electrode of Co-Mn-Ni oxides improved the efficiency of the EO process, therefore, the process of producing electrodes coated with nano-metal oxides is considered a promising method in the process of removing pollutants.

Acknowledgments

The authors appreciate the supportive suggestions and technical assistance made by the staff of the Department of Chemical Engineering, College of Engineering-University of Baghdad.

REFERENCES

1. Abbas, R.N., Abbas, A.S. 2022. kinetics and energetic parameters study of phenol removal from aqueous solution by electro-fenton advanced oxidation using modified electrodes with PbO2 and graphene. Iraqi Journal of Chemical and Petroleum Engineering, 23(2), 1–8. https://doi.org/10.31699/IJCPE.2022.2.1
2. Abbas, Z.I., Abbas, A.S. 2019. Oxidative degradation of phenolic wastewater by electro-fenton process using MnO2-graphite electrode. Journal of Environmental Chemical Engineering, 7(3), 103108. https://doi.org/10.1016/j.jece.2019.103108
3. Abilaji, S., Narenkumar, J., Das, B.S.S., Rajakrishnan, R., Sathishkumar, K., Rajamohan, R., Rajasekar, A. 2023. Electrochemical oxidation of azo dyes degradation by RuO2–IrO2–TiO2 electrode with biodegradation Aeromonas hydrophila AR1 and its degradation pathway: An integrated approach. Chemosphere, 345, 140516. https://doi.org/10.1016/j.chemosphere.2023.140516
4. Ahmed, Y.A., Salman, R.H. 2023a. Simultaneous electrodeposition of multicomponent of Mn–Co–Ni oxides electrodes for phenol removal by anodic oxidation. Case Studies in Chemical and Environmental Engineering, 8, 100386. https://doi.org/10.1016/j.cscee.2023.100386
5. Ahmed, Y.A., Salman, R.H. 2023b. Synthesis of Mn-Co-Ni composite electrode by anodic and cathodic electrodeposition for indirect electro-oxidation of phenol – optimization of the removal by response surface methodology. Ecological Engineering & Environmental Technology, 24(8), 107–119. https://doi.org/10.12912/27197050/171626
6. Ahmed, Z., Asghar, M.M., Malik, M.N., Nawaz, K. 2020. Moving towards a sustainable environment: The dynamic linkage between natural resources, human capital, urbanization, economic growth, and ecological footprint in China. Resources Policy, 67, 101677. https://doi.org/10.1016/j.resourpol.2020.101677
7. Akhtar, A., Aslam, Z., Asghar, A., Bello, M.M., Raman, A.A.A. 2020. Electrocoagulation of congo red dye-containing wastewater: Optimization of operational parameters and process mechanism. Journal of Environmental Chemical Engineering, 8(5), 104055. https://doi.org/10.1016/j.jece.2020.104055
8. Al-Qodah, Z., Al-Shannag, M. 2017. Heavy metal ions removal from wastewater using electrocoagulation processes: A comprehensive review. Separation Science and Technology, 1–28. https://doi.org/10.1080/01496395.2017.1373677
9. Ali, H.Q., Mohammed, A.A. 2020. Elimination of congo red dyes from aqueous solution using eichhornia crassipes. Iraqi Journal of Chemical and Petroleum Engineering, 21(4), 21–32. https://doi.org/10.31699/IJCPE.2020.4.3
10. Bafana, A., Devi, S.S., Chakrabarti, T. 2011. Azo dyes: past, present and the future. Environmental Reviews, 19(NA), 350–371. https://doi.org/10.1139/a11-018
11. Beddai, A.A., Badday, B.A., Al-Yaqoobi, A.M., Mejbel, M.K., Al Hachim, Z.S., Mohammed, M.K.A. 2022. Color removal of textile wastewater using

electrochemical batch recirculation tubular upflow cell. International Journal of Chemical Engineering, 2022, 1–8. https://doi.org/10.1155/2022/4713399

12. Chakawa, S., Aziz, M. 2021. Investigating the result of current density, temperature, and electrolyte concentration on cod: Subtraction of petroleum refinery wastewater using response surface methodology. Water (Switzerland), 13(6). https://doi.org/10.3390/w13060835
13. Chakchouk, I., Elloumi, N., Belaid, C., Mseddi, S., Chaari, L., Kallel, M. 2017. A combined electrocoagulation-electrooxidation treatment for dairy wastewater. Brazilian Journal of Chemical Engineering, 34(1), 109–117. https://doi.org/10.1590/0104-6632.20170341s20150040
14. Chanikya, P., Nidheesh, P.V., Syam Babu, D., Gopinath, A., Suresh Kumar, M. 2021. Treatment of dyeing wastewater by combined sulfate radical based electrochemical advanced oxidation and electrocoagulation processes. Separation and Purification Technology, 254, 117570. https://doi.org/10.1016/j.seppur.2020.117570
15. Chen, X., Ren, P., Li, T., Trembly, J.P., Liu, X. 2018. Zinc removal from model wastewater by electrocoagulation: Processing, kinetics and mechanism. Chemical Engineering Journal, 349, 358–367. https://doi.org/10.1016/j.cej.2018.05.099
16. Chen, X., Wang, S., Qiao, G., Lu, G., Cui, H., Wang, X. 2020. Fabrication of Three-Dimensional Porous NiO/Amorphous Ni(OH) 2 Composites for Supercapacitors. Energy & Fuels, 34(12), 16783–16790. https://doi.org/10.1021/acs.energyfuels.0c02767
17. Chen, Y., Hong, L., Xue, H., Han, W., Wang, L., Sun, X., Li, J. 2010. Preparation and characterization of TiO2-NTs/SnO2-Sb electrodes by electrodeposition. Journal of Electroanalytical Chemistry, 648(2), 119–127. https://doi.org/10.1016/j.jelechem.2010.08.004
18. Criado, S.P., Gonçalves, M.J., Ballod Tavares, L.B., Bertoli, S.L. 2020. Optimization of electrocoagulation process for disperse and reactive dyes using the response surface method with reuse application. Journal of Cleaner Production, 275, 122690. https://doi.org/10.1016/j.jclepro.2020.122690
19. Crini, G., Lichtfouse, E. 2019. Advantages and disadvantages of techniques used for wastewater treatment. Environmental Chemistry Letters, 17(1), 145–155. https://doi.org/10.1007/s10311-018-0785-9
20. El Boraei, N.F., Ibrahim, M. A.M. 2019. Black binary nickel cobalt oxide nano-powder prepared by cathodic electrodeposition; characterization and its efficient application on removing the Remazol Red textile dye from aqueous solution. Materials Chemistry and Physics, 238, 121894. https://doi.org/10.1016/j.matchemphys.2019.121894
21. Ganash, A., Alajlani, L., Ganash, E., Al-Moubaraki, A. 2023. Efficient electrochemical degradation of congo red dye by Pt/CuNPs electrode with its attractive performance, energy consumption, and mechanism: Experimental and theoretical approaches. Journal of Water Process Engineering, 56, 104497. https://doi.org/10.1016/j.jwpe.2023.104497
22. Inamuddin, Ahamed, M.I., Lichtfouse, E., Asiri, A. M. (Eds.). 2021. Green Adsorbents to Remove Metals, Dyes and Boron from Polluted Water (Vol. 49). Springer International Publishing. https://doi.org/10.1007/978-3-030-47400-3
23. Jia, Y., Ding, L., Ren, P., Zhong, M., Ma, J., Fan, X. 2020. Performances and mechanism of methyl orange and congo red adsorbed on the magnetic ion-exchange resin. Journal of Chemical & Engineering Data, 65(2), 725–736. https://doi.org/10.1021/acs.jced.9b00951
24. John, A., Saeed, A., Khan, Z. A. 2023. Influence of the duty cycle of pulse electrodeposition-coated Ni-Al2O3 Nanocomposites on Surface Roughness Properties. Materials, 16(6), 2192. https://doi.org/10.3390/ma16062192
25. Kabdaşlı, I., Tünay, O. 2023. Hexavalent Chromium Removal from Water and Wastewaters by Electrochemical Processes: Review. Molecules, 28(5), 2411. https://doi.org/10.3390/molecules28052411
26. Kapałka, A., Fóti, G., Comninellis, C. 2007. Kinetic modelling of the electrochemical mineralization of organic pollutants for wastewater treatment. Journal of Applied Electrochemistry, 38(1), 7–16. https://doi.org/10.1007/s10800-007-9365-6
27. Kaur, R., Kaur, H. 2016. Electrochemical degradation of Congo red from aqueous solution: role of graphite anode as electrode material. Portugaliae Electrochimica Acta, 34(3), 185–196.
28. Kul, M., Oskay, K.O., Erden, F., Akça, E., Katırcı, R., Köksaı, E., Akıncı, E. 2020. Effect of Process parameters on the electrodeposition of zinc on 1010 steel: Central composite design optimization. International Journal of Electrochemical Science, 15(10), 9779–9795. https://doi.org/10.20964/2020.10.19.
29. Kul, S., Boncukcuoğlu, R., Ekmekyapar Torun, F., Reçber, Z., Sözüdoğru, O., Aladağ, E. 2022. Investigation of the treatment of olive mill wastewater by electrooxidation. Water, Air, and Soil Pollution, 233(10), 421.
30. Li, A., Weng, J., Yan, X., Li, H., Shi, H., Wu, X. 2021. Electrochemical oxidation of acid orange 74 using Ru, IrO2, PbO2, and boron doped diamond anodes: Direct and indirect oxidation. Journal of Electroanalytical Chemistry, 898, 115622. https://doi.org/10.1016/j.jelechem.2021.115622.
31. Li, D., Ren, B., Jin, Q., Cui, H., Wang, C. 2018. Nitrogen-doped, oxygen-functionalized, edge- and defect-rich vertically aligned graphene for highly enhanced oxygen evolution reaction. Journal of Materials Chemistry A, 6(5), 2176–2183. https://doi.org/10.1039/C7TA07896J.

32. Mahmoodi, N.M., Taghizadeh, M., Taghizadeh, A. 2018. Mesoporous activated carbons of low-cost agricultural bio-wastes with high adsorption capacity: Preparation and artificial neural network modeling of dye removal from single and multicomponent (binary and ternary) systems. Journal of Molecular Liquids, 269, 217–228. https://doi.org/10.1016/j.molliq.2018.07.108.
33. Mandal, S., Calderon, J., Marpu, S.B., Omary, M.A., Shi, S.Q. 2021. Mesoporous activated carbon as a green adsorbent for the removal of heavy metals and congo red: characterization, adsorption kinetics, and isotherm studies. Journal of Contaminant Hydrology, 243, 103869. https://doi.org/10.1016/j.jconhyd.2021.103869.
34. Mohammadlou, N., Rasoulifard, M.H., Vahedpour, M., Eskandarian, M.R. 2014.The kinetic and thermodynamic study of decolorizing of congo red from aqueous solution using elctrogogulation process. Journal of Applied Chemical Research, 8(4), 123–144.https://sid.ir/paper/322943/en.
35. Moreira, F.C., Boaventura, R.A.R., Brillas, E., Vilar, V.J.P. 2017. Electrochemical advanced oxidation processes: A review on their application to synthetic and real wastewaters. Applied Catalysis B: Environmental, 202, 217–261. https://doi.org/10.1016/j.apcatb.2016.08.037.
36. Mousazadeh, M., Khademi, N., Kabdaşlı, I., Rezaei, S., Hajalifard, Z., Moosakhani, Z., Hashim, K. 2023. Domestic greywater treatment using electrocoagulation-electrooxidation process: optimisation and experimental approaches. Scientific Reports, 13(1), 15852. https://doi.org/10.1038/s41598-023-42831-6.
37. Nare, R.K., Ramesh, S., Basavi, P.K., Kakani, V., Bathula, C., Yadav, H.M., Dhanapal, P.B., Kotanka, R.K.R., Pasupuleti, V.R. 2022. Sonication-supported synthesis of cobalt oxide assembled on an N-MWCNT composite for electrochemical supercapacitors via three-electrode configuration. Scientific Reports, 12(1), 1998. https://doi.org/10.1038/s41598-022-05964-8.
38. Nasr, M., Ateia, M., Hassan, K. 2016. Artificial intelligence for greywater treatment using electrocoagulation process. Separation Science and Technology, 51(1), 96–105. https://doi.org/10.1080/01496395.2015.1062399.
39. Nidheesh, P.V., Zhou, M., Oturan, M.A. 2018. An overview on the removal of synthetic dyes from water by electrochemical advanced oxidation processes. Chemosphere, 197, 210–227. https://doi.org/10.1016/j.chemosphere.2017.12.195.
40. Ojo, T.A., Ojedokun, A.T., Bello, O.S. 2019. Functionalization of powdered walnut shell with orthophosphoric acid for congo red dye removal. Particulate Science and Technology, 37(1), 74–85.
41. Özyurt, B., Camcıoğlu, Ş., Hapoglu, H. 2017. A consecutive electrocoagulation and electro-oxidation treatment for pulp and paper mill wastewater. Desalination And Water Treatment, 93, 214–228. https://doi.org/10.5004/dwt.2017.21257.
42. Periyasamy, S., Muthuchamy, M. 2018. Electrochemical oxidation of paracetamol in water by graphite anode: Effect of pH, electrolyte concentration and current density. Journal of Environmental Chemical Engineering, 6(6), 7358–7367. https://doi.org/10.1016/j.jece.2018.08.036.
43. Ramya Sankar, M.S., Sivasubramanian, V. 2020. Application of statistical design to optimize the electrocoagulation of synthetic congo red dye solution and predicting the mechanism. International Journal of Environmental Science and Technology, 17(3), 1373–1386. https://doi.org/10.1007/s13762-019-02555-5.
44. Rathi, B.S., Kumar, P.S., Vo, D.V.N. 2021. Critical review on hazardous pollutants in water environment: Occurrence, monitoring, fate, removal technologies and risk assessment. Science of The Total Environment, 797, 149134. https://doi.org/10.1016/j.scitotenv.2021.149134
45. Ruoho, M., Niemelä, J.-P., Guerra-Nunez, C., Tarasiuk, N., Robertson, G., Taylor, A.A., Maeder, X., Kapusta, C., Michler, J., Utke, I. 2020. Thin-film engineering of mechanical fragmentation properties of atomic-layer-deposited metal oxides. Nanomaterials, 10(3), 558. https://doi.org/10.3390/nano10030558.
46. Sabah, I., Alwared, A.I. 2019. Adsorption of congo red dye from aqueous solution onto wheat husk in a fluidized bed reactor. Iraqi Journal of Chemical and Petroleum Engineering, 20(4), 55–60.
47. Salman, R.H., Abbar, A.H. 2023. Optimization of a combined electrocoagulation-electro-oxidation process for the treatment of Al-Basra Majnoon Oil field wastewater: Adopting a new strategy. Chemical Engineering and Processing - Process Intensification, 183, 109227. https://doi.org/10.1016/j.cep.2022.109227.
48. Sathishkumar, K., AlSalhi, M.S., Sanganyado, E., Devanesan, S., Arulprakash, A., Rajasekar, A. 2019. Sequential electrochemical oxidation and bio-treatment of the azo dye congo red and textile effluent. Journal of Photochemistry and Photobiology B: Biology, 200, 111655.
49. Sergienko, N., Radjenovic, J. 2020. Manganese oxide-based porous electrodes for rapid and selective (electro)catalytic removal and recovery of sulfide from wastewater. Applied Catalysis B: Environmental, 267, 118608. https://doi.org/10.1016/j.apcatb.2020.118608.
50. Shafqat, S.R., Bhawani, S.A., Bakhtiar, S., Ibrahim, M.N.M. 2020. Synthesis of molecularly

imprinted polymer for removal of congo red. BMC Chemistry, 14(1), 27. https://doi.org/10.1186/s13065-020-00680-8.

51. Siddiqui, S.I., Allehyani, E.S., Al-Harbi, S.A., Hasan, Z., Abomuti, M.A., Rajor, H.K., Oh, S. 2023. Investigation of congo red toxicity towards different living organisms: A review. Processes, 11(3), 807. https://doi.org/10.3390/pr11030807.
52. Tan, Y., Kang, Y., Wang, W., Lv, X., Wang, B., Zhang, Q., Cui, C., Cui, S., Jiao, S., Pang, G., Feng, S. 2021. Chitosan modified inorganic nanowires membranes for ultra-fast and efficient removal of Congo red. Applied Surface Science, 569, 150970. https://doi.org/10.1016/j.apsusc.2021.150970.
53. Theydan, S.K., Mohammed, W.T., Haque, S.M. 2024. Three-dimensional electrocoagulation process optimization employing response surface methodology that operated at batch recirculation mode for treatment refinery wastewaters. Iraqi Journal of Chemical and Petroleum Engineering, 25(1), 59–74. https://doi.org/10.31699/IJCPE.2024.1.6.
54. Turan, N. B. 2021. The application of hybrid electrocoagulation–electrooxidation system for the treatment of dairy wastewater using different electrode connections. Separation Science and Technology, 56(10), 1788–1801. https://doi.org/10.1080/01496395.2020.1788596.
55. Wu, W., Huang, Z.-H., Lim, T.-T. 2014. Recent development of mixed metal oxide anodes for electrochemical oxidation of organic pollutants in water. Applied Catalysis A: General, 480, 58–78. https://doi.org/10.1016/j.apcata.2014.04.035.
56. Ya, V., Martin, N., Choo, K.-H., Chou, Y.-H., Lee, S.-J., Le, N. C., Li, C.-W. 2019. High-pressure electrocoagulation system with periodic air replenishment for efficient dye wastewater treatment: Reaction dynamics and cost evaluation. Journal of Cleaner Production, 213, 1127–1134. https://doi.org/10.1016/j.jclepro.2018.12.249.
57. Zou, J., Peng, X., Li, M., Xiong, Y., Wang, B., Dong, F., Wang, B. 2017. Electrochemical oxidation of COD from real textile wastewaters: Kinetic study and energy consumption. Chemosphere, 171, 332–338. https://doi.org/10.1016/j.chemosphere.2016.12.065.